CHEMMEDCHEM

CHEMISTRY ENABLING DRUG DISCOVERY

Accepted Article

Title: Structure-based Design, Synthesis, and Biological Evaluation of Imidazo[4,5-b]pyridin-2-one-based p38 MAP Kinase Inhibitors: Part 1

Authors: Akira Kaieda, Masashi Takahashi, Hiromi Fukuda, Rei Okamoto, Shinji Morimoto, Masayuki Gotoh, Takahiro Miyazaki, Yuri Hori, Satoko Unno, Tomohiro Kawamoto, Toshimasa Tanaka, Sachiko Itono, Terufumi Takagi, Hiroshi Sugimoto, Kengo Okada, Gyorgy Snell, Ryan Bertsch, Jasmine Nguyen, Bi-Ching Sang, and Seiji Miwatashi

To be cited as: *ChemMedChem* 10.1002/cmdc.201900129

Link to VoR: http://dx.doi.org/10.1002/cmdc.201900129

A Journal of ChemPubSoc Europe

WILEY-VCH

www.chemmedchem.org

FULL PAPER WILEY-VCH

Structure-based Design, Synthesis, and Biological Evaluation of Imidazo[4,5-*b*]pyridin-2-one-based p38 MAP Kinase Inhibitors: Part 1

Akira Kaieda,*[a] Masashi Takahashi,[a] Hiromi Fukuda,[a] Rei Okamoto,[a] Shinji Morimoto,[a] Masayuki Gotoh,[a] Takahiro Miyazaki,[a] Yuri Hori,[a] Satoko Unno,[a] Tomohiro Kawamoto,[a] Toshimasa Tanaka,[a] Sachiko Itono,[a] Terufumi Takagi,[a] Hiroshi Sugimoto,[a] Kengo Okada,[a] Gyorgy Snell,[b] Ryan Bertsch,[b] Jasmine Nguyen,[b] Bi-Ching Sang,[b] and Seiji Miwatashi[a]

[a] A. Kaieda, M. Takahashi, H. Fukuda, R. Okamoto, S. Morimoto, M. Gotoh, T. Miyazaki, Y. Hori, S. Unno, T. Kawamoto, T. Tanaka, S. Itono, T. Takagi, H. Sugimoto, K. Okada, S. Miwatashi
Pharmaceutical Research Division, Takeda Pharmaceutical Company Limited., 26-1, Muraoka-higashi 2-chome, Fujisawa, Kanagawa 251-8555, Japan
E-mail: akira.kaieda@takeda.com
[b] G. Snell, R. Bertsch, J. Nguyen, B. Sang
Takeda California, 10410 Science Center Drive, San Diego, California 92121, United States

Abstract: We identified a lead series of p38 mitogen-activated protein kinase inhibitors using a structure-based design strategy from high-throughput screening of hit compound **1**. X-ray crystallography of **1** with the kinase showed an infrequent flip of the peptide bond between Met109 and Gly110, which was considered to lead to high kinase selectivity. Our structure-based design strategy was to conduct scaffold transformation of **1** with maintenance of hydrogen bond interactions with the flipped hinge backbone of the enzyme. In accordance with this strategy, we focused on scaffold transformation to identify imidazo[4,5-*b*]pyridin-2-one derivatives as potent inhibitors of the p38 MAP kinase. Of the compounds evaluated, **21** was a potent inhibitor of the p38 MAP kinase, lipopolysaccharide-induced tumor necrosis factor-α (TNF-α) production in human monocytic leukemia cells, and TNF-α-induced production of interleukin-8 in human whole blood cells. Herein, we have described the discovery of potent and orally bioavailable imidazo[4,5-*b*]pyridin-2-one-based p38 MAP kinase inhibitors that suppressed cytokine production in a human whole blood cell-based assay.

Introduction

The p38α mitogen-activated protein (MAP) kinase, a member of the family of serine/threonine protein kinases, is widely expressed in endothelial, immune, and inflammatory cells and plays a critical role in the regulation of the biosynthesis of proinflammatory cytokines, including tumor necrosis factor-α (TNF-α), interleukin-1β, and interleukin-6.[1,2] Selective biological agents against each of these cytokines have proven efficacious for the treatment of inflammatory diseases, including rheumatoid arthritis (RA), psoriasis, and inflammatory bowel disease.[3,4] TNF-α monoclonal antibodies (infliximab[5-7], adalimumub[8,9]) and the TNF-α receptor fusion protein, etanercept[10], are currently used as effective anti-RA agents; these have shown good efficacy in patients with active RA as alternative treatments to disease modifying antirheumatic drugs (DMARDs).

The MAP kinases include extracellular signal-regulated kinase, c-JUN N-terminal kinase, and p38 MAP kinase. The analysis of differential expression, localization, and activation of these MAP kinases in synovial tissue and cells extracted from patients with rheumatoid arthritis (RA), indicated the overactivation of the p38α isoform within the inflammatory tissue.[11-13] Therefore, the development of p38 MAP kinase inhibitors has been considered a promising solution for RA treatment.[14-18]

Numerous preclinical studies have reported that the inhibition of p38 MAP kinase effectively suppressed TNF-α production both *in vitro* and *in vivo*, and multiple chemical classes of p38 MAP kinase inhibitors have been discovered (Figure 1, 2, and 3). Unfortunately, BIRB-796[19,20], Scio-469[19,21], BMS-582949[19,22], VX-702[19,23,24], Ro-4402257[19,25], and TAK-715[16,26] have been discontinued, mainly owing to lack of efficacy. However, other inhibitors, including VX-745[19,27], BCT-197, LY-2228820, GW856553[19,28,29], PH-797804, AZD-7624, CHF-6297, FX-005, and ARRY-797[19], have been examined in Phase II clinical trials.[30]

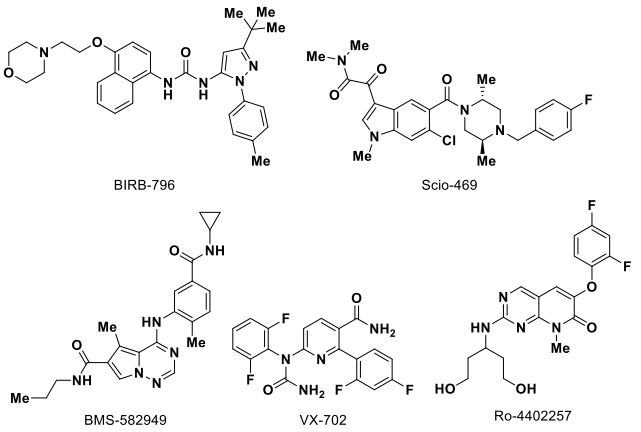

Figure 1. Representative discontinued p38 MAP kinase inhibitors.

The p38α also plays a central regulatory in the production of proinflammatory cytokines from microglia in the central nervous system (CNS). Human genetic studies and other biologic data suggest that the major drivers of Alzheimer's disease (AD) include dysregulated microglia[31,32] and

neuroinflammation[33,34]. In cognitively-impaired aged rats, VX-745 resulted in improved performance in the Morris water maze (MWM) test for cognitive performance.[35] The clinical development of VX-745 for the treatment of AD was recently started. Therefore, the inhibition of p38 MAP kinase is an attractive therapeutic target, for not only peripheral inflammation diseases, but also CNS diseases such as AD.

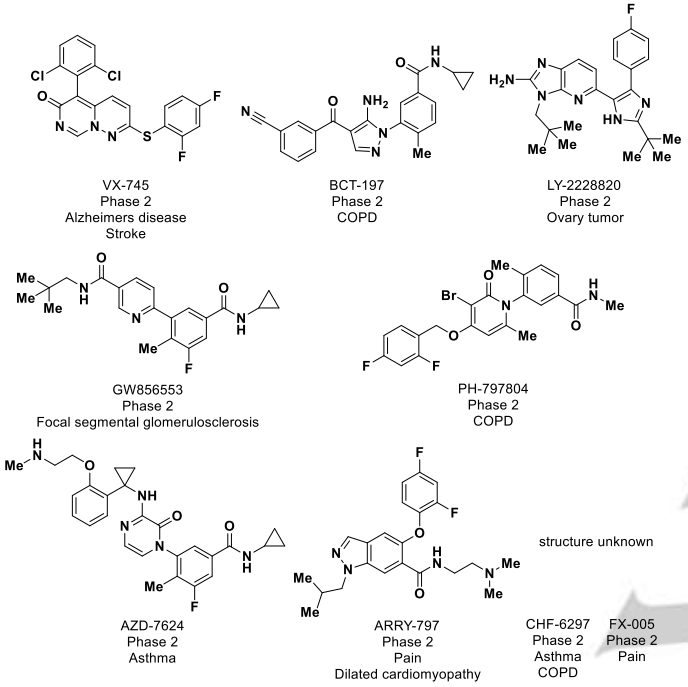

Figure 2. p38 MAP kinase inhibitors in Phase II clinical trials.

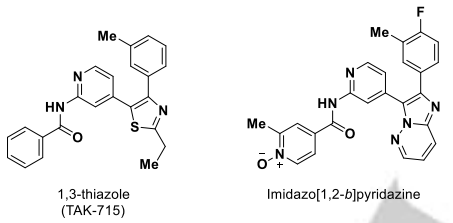

Figure 3. Structure of 1,3-thiazole and imidazo[1,2-*b*]pyridazine derivatives as p38 MAP kinase inhibitors.

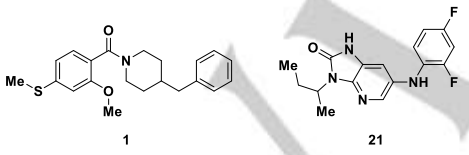

Figure 4. Structure of HTS hit **1** and lead compound **21** as p38 MAP kinase inhibitors.

We have previously reported the design and synthesis of p38 MAP kinase inhibitors based on 1,3-thiazole[16] and imidazo[1,2-*b*]pyridazine[26] (Figure 3). In our continued efforts to discover alternative classes of p38 MAP kinase inhibitors, we conducted high-throughput screening for p38 MAP kinase inhibition and identified a hit compound **1** (IC_{50} = 140 nM) with a completely different structure from the 1,3-thiazole or imidazo[1,2-*b*]pyridazine series (Figure 4). The hit compound **1** was successfully co-crystallized with the ATP binding domain of p38 MAP kinase (Figure 5). On the basis of the three-dimensional structure of the protein-ligand complex, we applied a structure-based approach for designing novel type of p38 MAP kinase inhibitors. For the inhibition of p38 MAP kinase, it is known that there is often a hydrogen bonding interaction observed between the inhibitor and the main chain amino acid in the hinge region of the ATP binding site; specifically, between the carbonyl oxygen and N-H of Met109[36]. Furthermore, in the co-crystal structure of the complex of compound **1** with p38 MAP kinase, unusual hydrogen bonding interaction between **1** and the hinge region was observed. Herein, we have reported a series of imidazo[4,5-*b*]pyridin-2-ones with greatly improved in vitro potency and bioavailability based on the design of compound **1**. From the X-ray crystallographic analysis of the complex of **1** bound to p38 MAP kinase, we designed and synthesized a series of scaffolds with hydrogen bonding acceptors able to interact with Met109 and Gly110 in a bidentate manner (Figure 6). Through scaffold hopping and SAR study, compound **21** was identified as a lead which exhibited excellent enzymatic inhibitory activity (IC_{50} = 9.6 nM) and potent cellular activity, with good oral bioavailability in rats. In this article, the design, synthesis, and biological activity of imidazo[4,5-*b*]pyridin-2-one derivatives are described as a lead series for another part of our overall strategy to advance multiple p38 MAP kinase inhibitors with various scaffolds.

Results and Discussion

High-throughput screening hit **1** showed moderate p38 inhibitory activity (IC_{50} = 140 nM) and was successfully co-crystallized with the ATP binding domain of the p38 MAP kinase (Figure 5). At a resolution of 1.80 Å, the co-crystal structure of **1** bound to p38 MAP kinase suggested that the carbonyl group of **1** interacted with the enzyme through two hydrogen bonds with the backbone amide of Met109 and Gly110 and that the hinge backbone conformation was different from that typically seen in protein kinases. Normally, the carbonyl of His107 and the NH and carbonyl of Met109 in the backbone are directed toward the ATP binding site and available for hydrogen bonding interactions with ligands. However, in this crystal structure, a flip of the peptide bond between Met109 and Gly110 led to a switching of the hydrogen-bond acceptor and donor distribution around the peptide plane. The peptide flip is considered energetically favorable because of the small size of the Gly110 side chain; bulkier residues would make the peptide flip much more energetically unfavorable.[36,37]

Only approximately 9.2% of all human protein kinases have glycine at the equivalent sequence position X + 4, where X is the gate-keeper residue.[37,38] It is supposed that the induction of the peptide-flipped hinge conformation is important for high kinase selectivity.[37] The hypothesis allowed the design of scaffold hopping with a cyclized carbonylpiperidine moiety, as shown in Figure 6. The benzimidazolone-based p38 MAP kinase inhibitors, initially reported by a research group at Boehringer Ingelheim, made our design attractive[39], while the carbonyl group only interacted with not Gly110 but Met109 of

the normal, not flipped, hinge backbone, and the NH group interacted with His107 of the normal hinge. This design of compound, with an exocyclic hydrogen binding acceptor, is intended to allow additional interaction with the carbonyl of His107; that is, hydrogen binding donor X can interact with His107. We therefore explored several scaffolds, i.e., oxindole, azaoxindole, benzimidazolone, or imidazopyridin-2-one with an exocyclic hydrogen binding acceptor able to interact with Met109 and Gly110 in a bidentate manner and to potentially lead to high kinase selectivity and discovered that imidazo[4,5-*b*]pyridin-2-one **2** resulted in moderate inhibition of the p38 MAP kinase (IC_{50} = 390 nM).

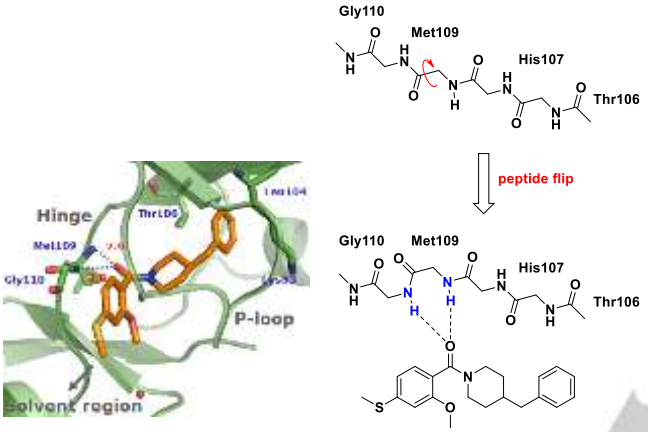

Figure 5. Binding interactions between **1** and p38 MAP kinase determined by X-ray crystallographic analysis (left: PDB code 6M95). Typical hinge conformation and binding mode of **1** with the peptide flipped hinge conformation (right).

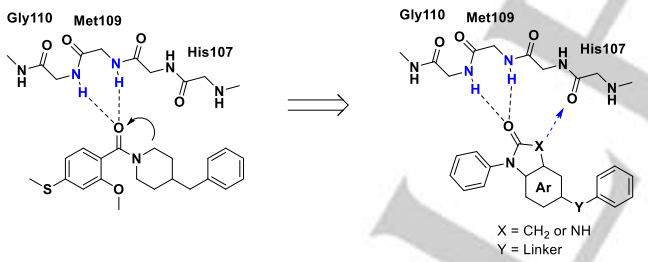

Figure 6. Scaffold hopping for discovery of new chemotypes.

The inhibitory potencies (IC_{50}) of the synthesized compounds were estimated by using a p38 MAP kinase assay (Table 1). As shown in Figure 5, the benzyl group is directed toward the shallow inner hydrophobic pocket defined by the residues Thr106 and Leu104. The previous research proved that the R^2 group was important for potent inhibitory activity and that smaller substituents, such as a methyl or fluoro group, were preferable.[16,26,38] Therefore, the introduction of small substituents for the R^2 group was focused on. Although the 3-methyl **3** showed much weaker inhibition of the p38 MAP kinase than **2**, the 2,4-difluoro derivative **4** exhibited more potent activity than **2**. Compared with **4**, the *ortho*-fluoro **5** showed more potent inhibition of the p38 MAP kinase, with an IC_{50} value of 27 nM. The replacement of the 2,4-difluorophenyl group in **5** with a 2,6-difluorophenyl group (**6**) led to a reduction in inhibitory activity. The *para*-fluoro group was therefore considered to be a good fit into the shallow pocket. In addition, the difluoro analogs **7** and **8** were synthesized and evaluated. Although the 2,4-difluoro compound **7** had lower inhibitory activity, the 2,6-difluoro compound **8** displayed more potent inhibitory activity against p38 than **5**. Furthermore, to confirm the effect of the *ortho*-substituent on the R^1 phenyl group, the 2,6-dichloro compound **9**, in which the fluoro groups were substituted for the chloro groups, was evaluated and was found to exhibit more potent inhibitory activity with an IC_{50} value of 5.6 nM. These results suggested that the steric effect of the *ortho*-position on the phenyl group as a R^1 substituent was important for potent inhibitory activity, rather than the electron withdrawing effect. It is of note that the phenyl group for R^1 and the imidazo[4,5-*b*]pyridin-2-one scaffold should be in mutually orthogonal planes. This consideration encouraged us to further explore substituent effects at the R^1 position. The benzyl compound **10** showed moderate inhibitory activity; however the phenethyl compound **11** reduced inhibitory activity compared with **4**. To control the direction of the phenyl group of the benzyl moiety of **10**, one or two methyl groups were introduced to the benzyl position (**12**, **13**). The mono-methyl substituted **12** showed tolerable inhibitory activity and the di-methyl substituted **13** showed decreased potency. A fluoro group, as an electron-withdrawing substituent, was introduced to the *ortho*-, *meta*-, or *para*-position (**14**-**16**) of the phenyl group of the benzyl moiety. Compared with **10**, the *meta*- and *para*-fluoro analogs **15** and **16** showed moderate potency and the *ortho*-fluoro **14** exhibited more potent inhibitory activity, with an IC_{50} value of 15 nM for the inhibition of the p38 MAP kinase. The introduction of another electron-withdrawing chloro group substituent (**17**) at an *ortho*-position on the phenyl group of the benzyl moiety reduced inhibitory activity to an IC_{50} value of 100 nM. This result suggested that the relatively small size of the fluorine atom was important for the inhibitory activity against the p38 MAP kinase. The 2,6-difluoro compound **18** slightly increased inhibitory activity, with an IC_{50} value of 12 nM. As the mono-substituted compound **12** was tolerable and the di-substituted compound **13** showed reduced activity, we explored some branched alkyl groups for R^1. The ^{i}propyl compound **19** exhibited more potent inhibitory activity than **12**, which suggested that the phenyl group at the R^1 position of **12** would be replaceable with the methyl group, which led to enhanced ligand efficiency. The ^{i}butyl compound **20** showed tolerable inhibitory activity, and the ^{s}butyl **21** and 3-pentyl **22** compounds had enhanced inhibitory activity against the p38 MAP kinase, with IC_{50} values of 9.6 and 6.7 nM, respectively. Given the properties of **20** and **21**, we determined that the methyl group at an adjacent position to the nitrogen atom would be effective for strong inhibitory activity against the p38 MAP kinase. This result also suggested that the branched alkyl group for R^1 and the imidazo[4,5-*b*]pyridin-2-one scaffold should be in mutually orthogonal planes. This was supported by the conformation of the benzyl group of **10**, as indicated in the X-ray crystal structure of the complex of **10** bound with the p38 MAP kinase (Figure 7).

As described in the introduction part, the development of the preceding multiple p38 MAP kinase inhibitors have often been discontinued due to lack of efficacy. Since not only strong enzyme inhibitory activity but also physicochemical properties are considered to be an important factor for a druglike lead

series, we analyzed structure-solubility relationship among these compounds (Table 1). The compounds **4**, **5**, **7** and **8** in which R^1 is an aryl group indicated a moderate solubility. The benzyl series **10** and **14**-**18** had relatively low solubility. On the other hand, it was found that the mono-methyl substituent on compound **12** greatly improved solubility. For the alkyl series, the isobutyl **20** was poorly-soluble, while isopropyl **19**, secondary butyl **21** and 3-pentyl **22** showed high solubility. From these facts, it was found that the water solubility tended to be higher when the adjacent position of the nitrogen on the imidazole ring was branched. It is worthy noted that the structural modification which leads to increase solubility is consistent with the direction in which the enzyme inhibitory activity enhances. Considering these observations, selected compounds were further evaluated on cellular level activity.

Table 1. Inhibitory activities of imidazo[4,5-*b*]pyridin-2-one derivatives against the p38 MAP kinase.

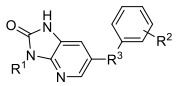

ID	R^1	R^2	R^3	IC_{50}[a] (nM)	Solubility[b] (μg/mL)
2	Ph	2-Me	NH	390 (330-470)	0.46
3	Ph	3-Me	NH	> 10000	0.34
4	Ph	2,4-diF	NH	63 (55-72)	4.7
5	2-F-Ph	2,4-diF	NH	27(24-30)	3.3
6	2-F-Ph	2,6-diF	NH	87 (76-99)	0.69
7	2,4-diF-Ph	2,4-diF	NH	100 (90-110)	4.5
8	2,6-diF-Ph	2,4-diF	NH	9.9 (8.9-11)	1.7
9	2,4-diCl-Ph	2,4-diF	NH	5.6 (4.9-6.4)	< 0.12
10	$PhCH_2$	2,4-diF	NH	29 (26-32)	1.8
11	$PhCH_2CH_2$	2,4-diF	NH	110 (90-120)	0.26
12	$PhCH(CH_3)$	2,4-diF	NH	31 (26-36)	10
13	$PhC(CH_3)_2$	2,4-diF	NH	150 (130-160)	3.0
14	2-F-$PhCH_2$	2,4-diF	NH	15 (13-16)	0.49
15	3-F-$PhCH_2$	2,4-diF	NH	37 (33-42)	1.8
16	4-F-$PhCH_2$	2,4-diF	NH	52 (44-60)	0.81
17	2-Cl-$PhCH_2$	2,4-diF	NH	100 (91-120)	0.14
18	2,6-diF-$PhCH_2$	2,4-diF	NH	12 (11-13)	0.11
19	^{i}Propyl	2,4-diF	NH	18 (16-19)	5.7
20	^{i}Butyl	2,4-diF	NH	26 (23-30)	0.69
21	^{s}Butyl	2,4-diF	NH	9.6 (8.5-11)	11
22	3-Pentyl	2,4-diF	NH	6.7 (6.0-7.5)	42
23	^{s}Butyl	2,4-diF	NCH_3	110 (92-120)	1.6
24	^{s}Butyl	2,4-diF	$NHCH_2$	9500 (8300-11000)	49

[a] The IC_{50} values shown are the mean values of quadruple measurements; the numbers in parentheses represent the 95% confidence intervals. [b] Solubility in pH = 6.8.

As indicated in Figure 7, the X-ray structure of the complex of **10** with the p38 MAP kinase, determined at 2.5 Å resolution, revealed that compound **10** binds to the p38 MAP kinase as expected. As observed in the crystal structure of hit compound **1** with p38, the exocyclic carbonyl oxygen of **10**

undergoes bidentate coordination with Met109 and Gly110 in the hinge region. Furthermore, the additional hydrogen bonding interaction between the NH hydrogen of imidazo[4,5-*b*]pyridin-2-one ring and the carbonyl oxygen of His107 was observed, as expected. The aniline hydrogen binds to Lys53 and Asp168 of the enzyme through water-mediated hydrogen bonding. In addition to these electrostatic interactions, the hydrophobic interaction of the R^2 groups contributes to the increased inhibition of p38, as shown by the SAR study (Table 1). The 2,4-difluorophenyl group fills the inner shallow hydrophobic pocket of the p38 MAP kinase consisting of Thr106 and Leu104. The SAR study of the R^1 groups suggests that increased lipophilicity of this part (**8**, **9**, **21**, and **22**) changes the orientation of R^1 substituents into the direction of hydrophobic pocket consisted of Ala157 and efficiently interact with protein surface compared with the benzyl group of **10** which does not occupy this pocket as shown in Figure 7. In a kinase panel study to probe potential off-target liabilities, while **1** showed negligible inhibition at 10 μM against 13 kinases, **8** and **22** exhibited excellent selectivity over 30 kinases (The evaluated kinase list and data for **1**, **8**, and **22** are given in the Supporting Information).

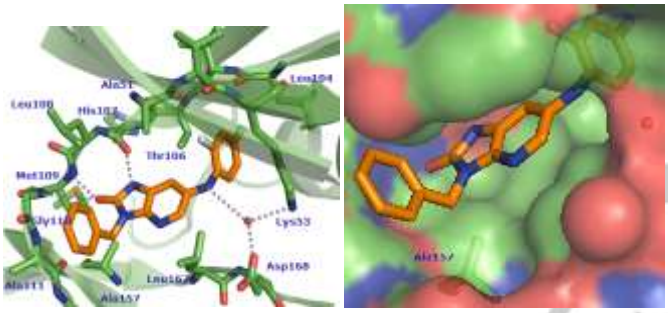

Figure 7. X-ray crystal structure of the complex of **10** and the p38 MAP kinase (left: PDB code 6M9L). Surface representation of the p38 MAP kinase illustrating the binding cavity. The inhibitor **10** is buried into this cavity. The pocket close to Ala157 is unoccupied by **10** (right).

The human monocytic leukemia cells (THP-1 cells) were used for the assessment of the effects of p38 MAP kinase inhibitors on cytokine production. In addition, the human whole blood (hWB) cell-based assay was conducted to evaluate the potential of the p38 inhibitors as a lead chemotype. It is supposed that suppression of cytokine production in the hWB assay reflects in vivo efficacy owing to the relative complexity of the cell-based assay. The inhibitory potencies (IC_{50}) of the representative compounds which were selected as the poorly or highly water soluble compounds with the potent enzymatic activities are summarized in Table 2. These compounds, **8**, **9**, **21**, and **22**, which showed similar inhibition of the p38 MAP kinase, inhibited the lipopolysaccharide (LPS)-induced production of TNF-α in THP-1 cells with IC_{50} values between 12–46 nM. The poorly-soluble aryl series **8** and **9** showed a slight decrease, in parallel, between p38 enzymatic inhibition and THP-1 cell-based inhibition; this was also seen in the highly-soluble alkyl series **21** and **22**. In addition, the compounds **8**, **9**, **21**, and **22** suppressed the TNF-α-induced production of interleukin-8 (IL-8) in hWB cells, but the potency of the highly-soluble alkyl series **21** and **22** was much greater than the poorly-soluble aryl series **8** and **9**. Although the explanation of this discrepancy between the aryl and alkyl series in the WB assay was unclear, it was considered that the physicochemical properties of **21** and **22** resulted in relatively potent activity in the WB cell-based assay due to contributions from their higher solubility as we anticipated. The pharmacokinetic properties of the lead compounds **21** and **22** in rats are shown in Table 3; higher oral exposure (AUC = 223.2 ng·h/mL) and bioavailability (*F*% = 49.2) was found for compound **21**, although lower oral exposure and bioavailability (AUC = 37.5 ng·h/mL; *F*% = 14.4) was found for compound **22**. The absorption and exposure of compound **21** were favorable in rats at a dose of 1 mg/kg and were sufficient for further study as a representative lead compound.

Table 2. The inhibitory activities of imidazo[4,5-*b*]pyridin-2-one derivatives on TNF-α production in human THP-1 cells, IL-8 production in human whole blood cells, and solubility.

ID	p38 IC_{50} (nM)	THP-1 IC_{50}[a] (nM)	hWB IC_{50}[a] (nM)	Solubility[b] (μg/mL)
8	9.9	36 (21-60)	93 (85-100)	1.7
9	5.6	21 (12-35)	200 (160-250)	< 0.12
21	9.6	46 (26-81)	15 (11-20)	11
22	6.7	12 (6.5-23)	20 (9.1-31)	42

[a] The IC_{50} values shown are the mean values of quadruple measurements; the numbers in parentheses represent the 95% confidence intervals. [b] Solubility in pH = 6.8.

Table 3. Pharmacokinetic parameters of **21** and **22** in rats[a].

ID	Cmax[b] (ng/mL)	Tmax[b] (h)	AUC[b] (n·gh/mL)	MRT[b] (h)	Vd (mL/kg)	CL (mL/h/kg)	*F* (%)
21	55.8	2.7	223.2	2.9	1894	2240	49.2
22	14.1	0.80	37.5	1.8	2905	3855	14.4

[a] Mean values of measurements conducted in three animals; i.v. 0.1 mg/kg, p.o. 1.0 mg/kg in 0.5% methyl cellulose suspension. [b] p.o. data.

Chemistry

The synthesis of imidazo[4,5-*b*]pyridin-2-one analogs **2–24** followed a general route, as outlined in Schemes 1–3 (experimental procedures for compounds **2–24** and intermediates are given in the supporting information). During the synthesis of the designed p38 MAP kinase inhibitors, we developed a highly regio-selective method of the introduction of amines into the tri-substituted pyridines **25** and **26**. In Scheme 1, chloropyridine **25** was treated with cesium fluoride to afford fluoropyridine **26**. Aromatic nucleophilic substitution reaction with the appropriate amines R^1NH_2 produced the corresponding compounds **27a–o**. For the introduction of the second amine, the Buchwald reaction using the appropriate amines R^2NH_2 led to the corresponding key intermediates **28a–s**. The subsequent alkaline hydrolysis of **28a–s** produced the carboxylic acids **29a–s** as a cyclization precursor. The final cyclization was successfully accomplished with treatment of **29a–s** with DPPA. The reaction mechanism of the cyclization step was considered to include multistep reactions, which consisted of the formation of acyl azide, the production of isocyanate via Curtius rearrangement, and intramolecular cyclization, in which the isocyanate was trapped by an adjacent amino group. As indicated in Scheme 2, for the introduction of the same substituent for the R^1 and R^2 groups, Buchwald reaction conditions using excess 2,4-difluoroaniline (more than 2 equivalents) with **26** afforded **28t**, which led to **7** in a similar manner to that described in Scheme 1. Next, we tried to change the order of the introduction of R^1 and R^2 groups. In Scheme 3, we succeeded in a highly regio-selective Buchwald reaction using Xantphos and $Pd_2(dba)_3$ as the catalysts to accomplish the synthesis of **30a–b** without any impact of the chloride group at the 2-position. The subsequent Buchwald reaction using BINAP and $Pd(OAc)_2$ as a catalyst produced the tri-substituted pyridines **28u–w** modified by the desired appropriate substituents. The tri-substituted pyridines **28u–w** led to the corresponding compounds **6**, **8**, and **9** in a similar manner to that described in Scheme 1.

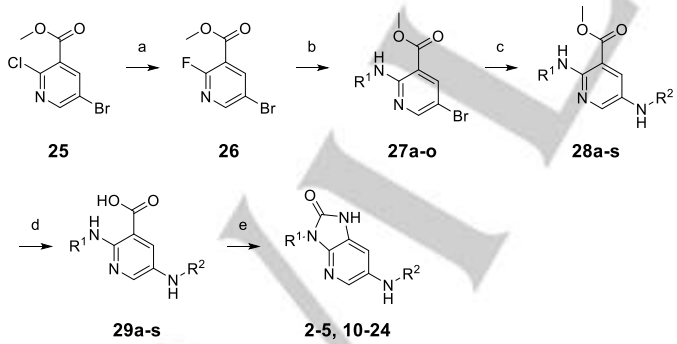

Scheme 1. Synthesis of compounds **2-5** and **10-24**. Reagents and conditions: (a) CsF, DMSO, 50 °C; (b) R^1NH_2, DMSO, 100 °C; (c) R^2NH_2, XPhos, $Pd_2(dba)_3$, Cs_2CO_3, toluene, 100 °C; (d) 1 N NaOH, THF-MeOH-H_2O, rt; (e) DPPA, Et_3N, toluene, 100 °C.

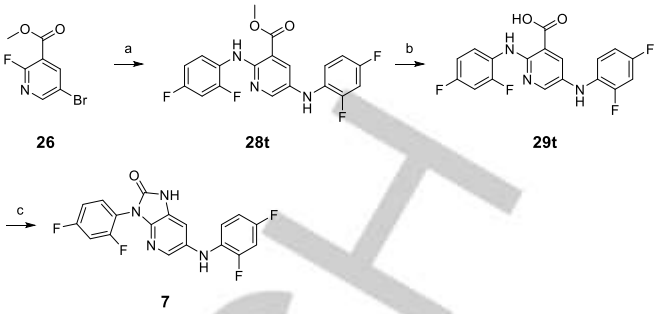

Scheme 2. Synthesis of compound **7**. Reagents and conditions: (a) 2,4-Difluoroaniline, Xphos, $Pd_2(dba)_3$, Cs_2CO_3, 60 °C; (b) 1 N NaOH, THF-MeOH-H_2O, rt; (c) DPPA, Et_3N, toluene, 100 °C.

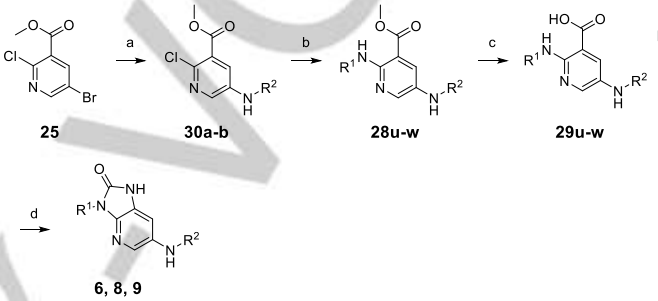

Scheme 3. Synthesis of compound **6**, **8**, and **9**. Reagents and conditions: (a) R^2NH_2, Xantphos, $Pd_2(dba)_3$, Cs_2CO_3, toluene, 100 °C; (b) R^1NH_2, BINAP, $Pd(OAc)_2$, Cs_2CO_3, toluene, MW, 150 °C; (c) 1 N NaOH, THF-MeOH-H_2O, rt; (d) DPPA, Et_3N, toluene, 100 °C.

Conclusions

Based on the X-ray crystallographic analysis of the complex of **1** with the p38 MAP kinase, we focused on the scaffold transformation of the carbonylpiperidine moiety of **1** while maintaining the binding mode in which **1** was coordinated in a bidentate manner. To investigate a scaffold with an exocyclic hydrogen binding acceptor, imidazo[4,5-*b*]pyridin-2-one derivatives were designed, synthesized, and identified as potent inhibitors of the p38 MAP kinase. Through the extensive SAR analysis and structure-solubility relationship analysis, compound **21** was discovered to exhibit excellent enzymatic inhibitory activity (IC_{50} = 9.6 nM), suppress IL-8 production in human WB cells (IC_{50} = 15 nM), and have good oral bioavailability in rats. Collectively, we identified that **21** was appropriate for further study as a lead compound of imidazo[4,5-*b*]pyridin-2-one-based p38 MAP kinase inhibitors.

Experimental Section

Chemistry: Melting points were determined with a Yanagimoto melting point apparatus or a Büchi melting point apparatus B-545 and are uncorrected. ^1H NMR spectra were obtained at 200 or 300 MHz on a Varian Gemini-200, a Varian Ultra-300, or a Bruker DPX-300 spectrometer. Chemical shifts are given in δ values (ppm) using

tetramethylsilane as the internal standard. Peak multiplicities are expressed as follows: s, singlet; d, doublet; t, triplet; q, quartet; dd, doublet of doublet; br, broad; brs, broad singlet; m, multiplet. Elemental analyses were carried out by Takeda Analytical Laboratories Ltd. Reactions were followed by TLC on Silica gel 60 F 254 precoated TLC plates (E. Merck) or NH TLC plates (Fuji Silysia Chemical Ltd.). Chromatographic separations were carried out on silica gel 60 (0.063–0.200 or 0.040–0.063 mm, E. Merck) or basic silica gel (Chromatorex® NH, 100–200 mesh, Fuji Silysia Chemical Ltd.) using the indicated eluents. Yields are unoptimized. Column chromatography was performed using Merck silica gel 60 (70–230 mesh). Thin-layer chromatography (TLC) was performed on Merck silica gel plates 60F254. LC-MS analysis was performed on a Shiseido CAPCELL PACK C-18 UG120 S-3 column (1.5 mmϕ × 35 mm) in a Waters Alliance 2795 or an Agilent 1100 LC system equipped with a Waters 2487 absorbance detector and a Micromass ZQ2000 mass spectrometer. Analytes were eluted using a linear gradient of water (0.05% TFA)/acetonitrile (0.04% TFA) from 90:10 to 0:100 over 4 min at a flow rate of 0.5 mL/min. UV detection was at 220 nm. Preparative HPLC was performed on a Shiseido CAPCELL PACK C-18 UG120 S-5 column (20 mmϕ × 50 mm), eluting at 25 mL/min with a gradient of water (0.1% TFA)/acetonitrile (0.1% TFA). UV detection was at 220 nm. The purity of all compounds used in biological studies was determined to be ≥ 95% by elemental analysis or a HPLC with Corona CAD (Charged Aerosol Detector), Nano quantity analyte detector (NQAD), or photo diode array detector. Elemental analyses were performed by Takeda Analytical Research Laboratories, Ltd. Experimentally determined hydrogen, carbon, and nitrogen composition by elemental analysis was within ±0.4% of the expected value, implying a purity of ≥ 95%. For a HPLC analysis, the column was a Capcell Pak C18AQ (50 mm × 3.0 mm ID, Shiseido, Japan) or L-column 2 ODS (30 mm × 2.0 mm ID, CERI, Japan) with a temperature of 50 °C and a flow rate of 0.5 mL/min. Mobile phases A and B under a neutral condition were a mixture of 50 mM ammonium acetate, H_2O, and CH_3CN (1:8:1, v/v/v) and a mixture of 50 mM ammonium acetate and CH_3CN (1:9, v/v), respectively. The ratio of mobile phase B was increased linearly from 5% to 95% over 3 min, 95% over the next 1 min. Mobile phases A and B under an acidic condition were a mixture of 0.2% formic acid in 10 mM ammonium formate and 0.2% formic acid in CH_3CN, respectively. The ratio of mobile phase B was increased linearly from 14% to 86% over 3 min, 86% over the next 1 min. All experiments using animals were reviewed and approved by the Internal Animal Care and Use Committee of Takeda Pharmaceutical Research Division. The experimental procedures for representative compounds **2**, **7** and **6** were as follows (experimental procedures for compounds **2–24** and intermediates are given in the supporting information).

Methyl 5-bromo-2-fluoropyridine-3-carboxylate (26). To a solution of methyl 5-bromo-2-chloropyridine-3-carboxylate (**25**) (100 g, 39.9 mmol) in DMSO (1.33 L) was added cesium fluoride (84.9 g, 559 mmol) at 45 °C. The mixture was stirred at 50 °C for 48 h and cooled to room temperature. To the mixture was added ethyl acetate. The mixture was washed with H_2O. The aqueous layer was extracted with ethyl acetate. The combined organic layers was washed with brine, dried over sodium sulfate, and concentrated in vacuo. The residue was purified by silica gel column chromatography (hexane: ethyl acetate= 100: 0- 50: 1) to give **26** as a white powder (81.3 g, 87%). ^{1}H NMR (300 MHz, DMSO-d_6) δ: 3.89 (3H, s), 8.56 (1H, dd, *J* = 8.2, 2.5 Hz), 8.66 (1H, dd, *J* = 2.6, 1.3 Hz).

Methyl 5-bromo-2-phenylaminopyridine-3-carboxylate (27a). A solution of **26** (577 mg, 2.47 mmol) and aniline (276 mg, 2.96 mmol) in DMSO (4 mL) was stirred at 100 °C for 15 h and cooled to room temperature. To the mixture was added H_2O. The resulting solid was collected on a filter, washed with H_2O, and dried under reduced pressure to give **27a** as a pale yellow powder (670 mg, 80%). ^{1}H NMR (300 MHz, DMSO-d_6) δ: 3.91 (3H, s), 7.07 (1H, t, *J* = 7.3 Hz), 7.29-7.39 (2H, m), 7.62-7.70 (2H, m), 8.33 (1H, d, *J* = 2.4 Hz), 8.51 (1H, d, *J* = 2.6 Hz), 10.01 (1H, s). MS (ESI+): 308 (M+H).

Methyl 2-anilino-5-(2-methylanilino)pyridine-3-carboxylate (28a). A solution of **27a** (307 mg, 1.0 mmol), 2-methylaniline (0.13 mL, 1.2 mmol), $Pd_2(dba)_3$ (9.2 mg, 0.01 mmol), Xphos (9.5 mg, 0.02 mmol), and cesium carbonate (652 mg, 2.0 mmol) in toluene (5 mL) was stirred at 100 °C for overnight under argon atmosphere. To the resulting mixture was added H_2O. The mixture was extracted with ethyl acetate, washed with H_2O and brine, dried over magnesium sulfate, and concentrated in vacuo. The residue was purified with a silica gel column chromatography (hexane: ethyl acetate= 10: 0- 2: 8) to give **28a** as a yellow powder (293 mg, 92%). ^{1}H NMR (300 MHz, DMSO-d_6) δ: 2.22 (3H, s), 3.83 (3H, s), 6.81 (1H, t, *J* = 7.3 Hz), 6.89-7.02 (2H, m), 7.16 (1H, d, *J* = 7.2 Hz), 7.23-7.36 (3H, m), 7.69 (2H, d, *J* = 7.5 Hz), 7.94 (1H, d, *J* = 3.0 Hz), 8.25 (1H, d, *J* = 3.0 Hz), 9.86 (1H, s).

2-Anilino-5-(2-methylanilino)pyridine-3-carboxylic acid (29a). A solution of **28a** (290 mg, 0.87 mmol) and 1N NaOH aqueous solution (3.57 mL, 3.57 mmol) in tetrahydrofuran (5 mL), methanol (5 mL) and H_2O (1 mL) was stirred at room temperature for 3 h. To the resulting mixture was added 1N HCl aqueous solution (3.57 mL, 3.57 mmol) at room temperature. After being concetrated in vacuo, the residue was diluted with ethyl acetate, washed with H_2O and brine, dried over magnesium sulfate, and concentrated in vacuo. The residue was purified with a silica gel column chromatography (hexane: ethyl acetate= 7: 3- 1: 9) to give **29a** as a yellow powder (120 mg, 43%). ^{1}H NMR (300 MHz, DMSO-d_6) δ: 2.23 (3H, s), 6.79 (1H, td, *J* = 7.3, 0.9 Hz), 6.90-6.99 (2H, m), 7.02-7.10 (1H, m), 7.15 (1H, d, *J* = 7.2 Hz), 7.22 (1H, s), 7.23-7.35 (2H, m), 7.69 (2H, d, *J* = 7.6 Hz), 7.94 (1H, d, *J* = 2.7 Hz), 8.21 (1H, d, *J* = 2.7 Hz), 10.23 (1H, brs), 13.60 (1H, brs).

6-(2-Methylanilino)-3-phenyl-1,3-dihydro-2*H*-imidazo[4,5-*b*]pyridin-2-one (2). A solution of **29a** (120 mg, 0.38 mmol), DPPA (0.084 mL, 0.39 mmol), and Et_3N (0.059 mL, 0.42 mmol) in toluene (10 mL) was stirred at 100 °C for 2 h. To the resulting mixture was added H_2O. The mixture was extracted with ethyl acetate, washed with H_2O and brine, dried over magnesium sulfate, and concentrated in vacuo. The residue was purified with a silica gel column chromatography (hexane: ethyl acetate= 7: 3- 4: 6) to give a brown powder. The powder was recrystallized from ethanol to give **2** as a pale white powder (75 mg, 62%). mp: 283–284 °C (ethanol). ^{1}H NMR (300 MHz, DMSO-d_6) δ: 2.22 (3H, s), 6.82-6.89 (1H, m), 6.96-7.13 (3H, m), 7.18 (1H, d, *J* = 7.5 Hz), 7.30-7.42 (2H, m), 7.52 (2H, t, *J* = 7.7 Hz), 7.63-7.76 (3H, m), 11.15 (1H, s). MS (ESI+): 317 (M+H). Anal. Calcd for $C_{19}H_{16}N_4O\cdot0.1H_2O$: C, 71.73; H, 5.13; N, 17.61. Found: C, 71.73; H, 5.01; N, 17.48.

2,5-Bis(2,4-difluoroanilino)pyridine-3-carboxylic acid (29t). A solution of **26** (300 mg, 1.3 mmol), 2,4-difluoroaniline (199 mg, 1.5

mmol), $Pd_2(dba)_3$ (11.7 mg, 0.01 mmol), Xphos (12.2 mg, 0.03 mmol), and cesium carbonate (835 mg, 2.6 mmol) in toluene (30 mL) was stirred at 100 °C for 15 h under argon atmosphere. To the mixture were added 2,4-difluoroaniline (199 mg, 1.5 mmol), $Pd_2(dba)_3$ (11.7 mg, 0.01 mmol), Xphos (12.2 mg, 0.03 mmol), and cesium carbonate (835 mg, 2.6 mmol). The mixture was stirred at 100 °C for 15 h under argon atmosphere. The mixture was filtered through celite pad. To the filtrate was added H_2O. The mixture was extracted with ethyl acetate, washed with H_2O and brine, dried over sodium sulfate, and concentrated in vacuo. The residue was purified with a silica gel column chromatography (hexane: ethyl acetate= 98: 2- 70: 30) to give methyl 2,5-bis(2,4-difluoroanilino)pyridine-3-carboxylate (**28t**) as a brown powder (127 mg, 25%), and used in the next reaction. This compound was prepared from **28t** as described in the synthesis of **29a** as a brown powder (122 mg, quant). ^{1}H NMR (300 MHz, DMSO-d_6) δ: 6.85-7.18 (3H, m), 7.19-7.43 (2H, m), 7.79 (1H, s), 7.92 (1H, d, *J* = 3.0 Hz), 8.16 (1H, d, *J* = 2.6 Hz), 8.44-8.62 (1H, m).

6-(2,4-Difluoroanilino)-3-(2,4-difluorophenyl)-1,3-dihydro-2*H*-imidazo[4,5-*b*]pyridin-2-one (7). This compound was prepared from **29t** as described in the synthesis of **2** as a white powder (7%). mp: 245–247 °C. ^{1}H NMR (300 MHz, DMSO-d_6) δ: 6.87-7.07 (2H, m), 7.12-7.35 (3H, m), 7.46-7.60 (1H, m), 7.60-7.73 (2H, m), 7.85 (1H, s), 11.26 (1H, s). MS (ESI+): 375 (M+H). HPLC purity: 100%.

Methyl 2-chloro-5-(2,6-difluoroanilino)pyridine-3-carboxylate (30a). A solution of **25** (1500 mg, 6.0 mmol), 2,6-difluoroaniline (0.831 mL, 7.2 mmol), $Pd_2(dba)_3$ (137 mg, 0.15 mmol), Xantphos (174 mg, 0.3 mmol), and cesium carbonate (6800 mg, 21 mmol) in toluene (20 mL) was stirred at 100 °C under nitrogen atmosphere for overnight. To the resulting mixture was added H_2O. The mixture was extracted with ethyl acetate, washed with H_2O and brine, dried over magnesium sulfate, and concentrated in vacuo. The residue was purified with a silica gel column chromatography (hexane: ethyl acetate= 4: 1) to give **30a** as a yellow powder (896 mg, 50%). ^{1}H NMR (300 MHz, DMSO-d_6) δ: 3.84 (3H, s), 7.16-7.35 (3H, m), 7.39-7.46 (1H, m), 8.03 (1H, d, *J* = 3.0 Hz), 8.62 (1H, s). MS (ESI+): 299 (M+H).

Methyl 5-(2,6-difluoroanilino)-2-(2-fluoroanilino)pyridine-3-carboxylate (28u). A solution of **30a** (448 mg, 1.5 mmol), 2-fluoroaniline (0.174 mL, 1.8 mmol), palladium acetate (16.8 mg, 0.075 mmol), BINAP (56.0 mg, 0.090 mmol), and cesium carbonate (1220 mg, 3.8 mmol) in toluene (10 mL) was stirred at 150 °C under microwave radiation for 2 h. After being cooled to room temperature, the mixture was diluted with ethyl acetate and filtered through celite pad. The filtrate was washed with H_2O and brine, dried over sodium sulfate, and concentrated in vacuo. The residue was purified with a silica gel column chromatography (hexane: ethyl acetate= 4: 1) to give **28u** as a yellow powder (466 mg, 83%). ^{1}H NMR (300 MHz, DMSO-d_6) δ: 3.88 (3H, s), 6.90-7.05 (1H, m), 7.08-7.32 (5H, m), 7.70 (1H, d, *J* = 2.7 Hz), 8.03 (1H, s), 8.10 (1H, d, *J* = 2.7 Hz), 8.56 (1H, dt, *J* = 8.3, 1.5 Hz), 10.07 (1H, d, *J* = 3.4 Hz). MS (ESI+): 374 (M+H).

5-(2,6-Difluoroanilino)-2-(2-fluoroanilino)pyridine-3-carboxylic acid (29u). This compound was prepared from **28u** as described in the synthesis of **29a** as a yellow powder (quant). ^{1}H NMR (300 MHz, DMSO-d_6) δ: 6.87-7.01 (1H, m), 7.06-7.29 (5H, m), 7.65-7.72 (1H, m), 7.99 (1H, s), 8.07 (1H, d, *J* = 3.0 Hz), 8.59 (1H, td, *J* = 8.3, 1.5 Hz), 10.35 (1H, brs), 13.69 (1H, brs). MS (ESI+): 360 (M+H).

6-(2,6-Difluoroanilino)-3-(2-fluorophenyl)-1,3-dihydro-2*H*-imidazo[4,5-*b*]pyridin-2-one (6). This compound was prepared from **29u** as described in the synthesis of **2** as a white powder (44%). mp: 296–297 °C. ^{1}H NMR (300 MHz, DMSO-d_6) δ: 6.78 (1H, s), 7.08-7.25 (3H, m), 7.27-7.67 (5H, m), 7.95 (1H, s), 11.16 (1H, s). MS (ESI+): 357 (M+H). Anal. Calcd for $C_{18}H_{11}N_4F_3O$: C, 60.68; H, 3.11; N, 15.72. Found: C, 60.39; H, 3.21; N, 15.53.

Biology: p38 MAP kinase enzyme assay: The FLAG-tagged human p38α protein was expressed with a baculovirus system and activated by constitutive active human MKK3. Then, the recombinant p38α protein was purified using the anti-FLAG antibody affinity agarose gel (Sigma). Kinase reactions were evaluated with LanthaScreen assay system (Life Technologies, USA); 2.5 µL of test compounds, diluted with DMSO (final concentration 1% DMSO), were added to the reaction mixture (25 mM HEPES [pH7.5], 10 mM Mg acetate, 1 mM DTT, 0.01% Tween-20, and 0.01% BSA) containing 125 pg human p38α protein and 8 nM GFP-ATF2 (19-96) (Life Technologies) in 384-well plates (Nunc, USA). After a 5 min incubation at room temperature, the reaction was started by adding 5 µL of 580 µM ATP. After a 20 min incubation, the reaction was terminated by adding 5 µL of 80 mM EDTA. Then, 5 µL of the Tb-anti-phospho ATF2 (pThr71) antibody (Life Technologies) was added and incubated for 60 min at room temperature. The time-resolved fluorescence resonance energy transfer (TR-FRET) signal was measured using EnVision Multilabel Plate Reader (PerkinElmer).

TNF-α production assay in THP-1 cells: THP-1 cells were suspended in RPMI 1640 medium (Life Technologies) containing 1% fetal bovine serum (Morgate, Australia). Then, 40 µL of the cell suspension ($0.625X10^6$ cells/mL) was added to 384-well plates (Corning, USA) and mixed with 5 µL of test compounds diluted with 10% DMSO. After 60 min incubation at 37 °C and 5% CO_2, the cells were stimulated with 5 µL of 100 µg/mL LPS (Wako). After incubating for 4 h at 37°C and 5% CO_2, the concentration of TNF-α in the medium was measured with the TNF-α HTRF kit (CisBio, USA). The TR-FRET signal was measured with EnVision Multilabel Plate Reader (PerkinElmer).

TNF-α production assay in human whole blood cells: Human whole blood was diluted with RPMI 1640 medium (Nikken-bio) to be 2.5 times. Then, 160 µL of the diluted blood was added to 96-well plates and mixed with 20 µL of test compounds diluted with 10% DMSO. After 60 min incubation at 37 °C and 5% CO_2, the blood was stimulated with 20µL of 300 ng/mL human TNF-α. After incubating for 18-24 h at 37°C and 5% CO_2, the concentration of IL-8 in the medium was measured with the IL-8 ELISA kit (R&D systems, USA). The absorbance was measured with Wallac 1420 Plate Reader (PerkinElmer).

Solubility: Small volumes of the compound solution dissolved in DMSO were added to the aqueous buffer solution (pH 6.8). After incubation, precipitates were separated by filtration. The solubility was determined by HPLC analysis of each filtrate.

Pharmacokinetics: Rat cassette BA: Test compounds were administered intravenously (0.1 mg/kg) or orally (1 mg/kg) by cassette dosing to non-fasted rats. After administration, blood samples were collected and centrifuged to obtain the plasma fraction. The plasma samples were deproteinized by mixing with acetonitrile followed by centrifugation. The compound concentrations in the supernatant were measured by LC-MS/MS.

Acknowledgements ((optional))

The authors thank Drs. Shigenori Ohkawa, Yuji Ishihara, Fumio Itoh, Osamu Uchikawa and Yoshinori Ikeura for their valuable discussions of this work, and Drs. Takashi Ichikawa and Shinichiro Matsunaga for their critical review of the manuscript. We also thank the members of the Takeda Analytical Research Laboratories, Ltd. for elemental analyses. We would like to thank the staff at the Berkeley Center for Structural Biology, Lawrence Berkeley National Laboratory, which operates the Advanced Light Source beamline 5.0.3, where the x-ray diffraction data was collected. The Berkeley Center for Structural Biology is supported in part by the National Institutes of Health, National Institute of General Medical Sciences, and the Howard Hughes Medical Institute. The Advanced Light Source is a Department of Energy Office of Science User Facility under Contract No. DE-AC02-05CH11231.

Keywords: p38 mitogen-activated protein kinase inhibitors • rheumatoid arthritis • structure-based design • imidazo[4,5-*b*]pyridin-2-one derivatives

References:

[1] Schett, G.; Zwerina, J.; Firestein, G. The p38 mitogen-activated protein kinase (MAPK) pathway in rheumatoid arthritis. *Ann. Rheum. Dis.* **2008**, *67*, 909–916.

[2] Westra, J.; Limburg, P. C. p38 mitogen-activated protein kinase (MAPK) in rheumatoid arthritis. *Mini-Rev. Med. Chem.* **2006**, *6*, 867–874.

[3] Schett, G.; Stach, C.; Zwerina, J.; Voll, R.; Manger, B. How antirheumatic drugs protect joints from damage in rheumatoid arthritis. *Arthritis Rheum.* **2008**, *58*, 2936–2948.

[4] Strand, V.; Singh, J. A. Improved health-related quality of life with effective disease-modifying antirheumatic drugs: evidence from randomized controlled trials. *Am. J. Manag. Care* **2008**, *14*, 234–254.

[5] Elliott, M. J.; Cerami, N. M.; Feldmann, M.; Kalden, J. R.; Antoni, C.; Smolen, J. S.; Leeb, B.; Breedveld, F. C.; Macfarlane, J. D.; Biji, H.; Woody, J. N. Randomized double-blind comparison of chieric monoclonal antibody to tumor necrosis factor α (cA2) versus placebo in rheumatoid arthritis. *Lancet* **1994**, *344*, 1105-1110.

[6] Rankin, C. C.; Choy, E. H. S.; Kassimos, D.; Kingsley, G. H.; Sopwith, A. M.; Isenberg, D. A.; Panayi, G. S. The therapeutic effects of an engineered human anti-tumor necrosis factor alpha antibody (CDP571) in rheumatoid arthritis. *Br. J. Rheumatol.* **1995**, *34*, 334-342.

[7] Van Dullemann, H. M.; Van Deventers, S. J.; Hommens, D. W.; Biji, H.; Jansen, J.; Woody, J. N. Treatment of Crohn's Disease with Antitumor Necrosis Factor Chimeric Monoclonal Antibody (cA2). *Gastroenterology* **1995**, *109*, 129-135.

[8] Patel, T.; Gordon, K. B. Adalimumab: efficacy and safety in psoriasis and rheumatoid arthritis. *Dermatol Ther.* **2004**, *17*, 427-431.

[9] Bang, L. M.; Keating, G. M. Adalimumab: a review of its use rheumatoid arthritis. *BioDrugs.* **2004**, *18*, 121-139.

[10] Moreland, L. W.; Baumgartner, S. W.; Schiff, M. H.; Tindall, E. A.; Fleischmann, R. M.; Weaver, A. L.; Ettlinger, R. E.; Cohen, S.; Koopman, W. J.; Mohler, K.; Widmer, M. B.; Blosch, C. M. Treatment of rheumatoid arthritis with a recombinant human tumor necrosis factor receptor (p75)-Fe fusion protein. *N. Engl. J. Med.* **1997**, *337*, 141-147.

[11] Hale, K. K.; Trollinger, D.; Rihanek, M.; Manthey, C. L. Differential expression and activation of p38 mitogen-activated protein kinase alpha, beta, gamma, and delta in inflammatory cell lineages. *J. Immunol.* **1999**, *162*, 4246–4252.

[12] Korb, A.; Tohidast-Akrad, M.; Cetin, E.; Axmann, R.; Smolen, J.; Schett, G. Differential tissue expression and activation of p38 MAPK alpha, beta, gamma, and delta isoforms in rheumatoid arthritis. *Arthritis Rheum.* **2006**, *54*, 2745–2756.

[13] Schett, G.; Tohidast-Akrad, M.; Smolen, J. S.; Schmid, B. J.; Steiner, C. W.; Bitzan, P.; Zenz, P.; Redlich, K.; Xu, Q.; Steiner, G. Activation, differential localization, and regulation of the stress-activated protein kinases, extracellular signal-regulated kinase, c-JUN N-terminal kinase, and p38 mitogen-activated protein kinase, in synovial tissue and cells in rheumatoid arthritis. *Arthritis Rheum.* **2000**, *43*, 2501–2512.

[14] Goldstein, D. M.; Gabriel, T. Pathway to the clinic: inhibition of P38 MAP kinase. A review of ten chemotypes selected for development. *Curr. Top. Med. Chem.* **2005**, *5*, 1017–1029.

[15] Pettus, L. H.; Wurz, R. P. Small molecule p38 MAP kinase inhibitors for the treatment of inflammatory diseases: novel structures and developments during 2006-2008. *Curr. Top. Med. Chem.* **2008**, *8*, 1452–1467.

[16] Miwatashi, S.; Arikawa, Y.; Kotani, E.; Miyamoto, M.; Naruo, K.; Kimura, H.; Tanaka, T.; Asahi, S.; Ohkawa, S. Novel Inhibitor o p38 MAP Kinase as an Anti-TNF-α drug: Discovery of N-[4-[2-ethyl-4-(3-methylphenyl)-1,3-thiazol-5-yl]-2-pyridyl]benzamide (TAK-715) as a Potent and Orally Active Anti-rheumatoid Arthritis Agent. *J. Med. Chem.* **2005**, *48*, 5966-5979.

[17] Zlokarnik, G.; Grootenhuis, P. D. J.; Watson, J. B. High Throughput P450 Inhibition Screens in Early Drug Discovery. *Drug Discov. Today* **2005**, *10*, 1443-1450.

[18] Halgren, T. A. MMFF VI. MMFF94s Option for Energy Minimization Studies. *J. Comput. Chem.* **1999**, *20*, 720–729.

[19] Goldstein, D. M.; Kuglstatter, A.; Lou, Y.; Soth, M. J. Selective p38α Inhibitors Clinically Evaluated for the Treatment of Chronic Inflammatory Disorders. *J. Med. Chem.* **2010**, *53*, 2345-2353.

[20] Regan, J. R.; Breitfelder, P.; Cirillo, P.; Gilmore, T.; Graham, A. G.; Hickey, E.; Klaus, B.; Madwed, J.; Moriaki, M.: Moss, N.; Pargellis, C.; Pav, S.; Proto, A.; Tong, L.; Torcellini, C. Pyrazole urea-based inhibitors of p38 MAP Kinase: From lead compound to clinical candidate. *J. Med. Chem.* **2002**, *45*, 2994-3008.

[21] Tong, M. D.; Daniels, D. O.; Montano, T.; Chang, S.; Desjardins, P. SCIO-469, a novel p38a MAPK Inhibitors, provides efficacy in acute postsurgical dental pain. *Clin. Pharm. Ther.* **2004**, *75*, P3.

[22] Liu, C.; Lin, J.; Wrobleski, S. T.; Lin, S.; Hynes, J.; Wu, H.; Dyckman, A. J.; Li, T.; Wityak, J.; Gillooly, K. M.: Pitt, S.; Shen, D. R.; Zhang, R. F.; McIntyre, K. W.; Salter-Cid, L.; Shuster, D. J.; Zhang, H.; Marathe, P. H., Doweyko, A. M.; Sack, J. S.; Kiefer, S. E.; Kish, K. F.; Newitt, J. A.; McKinnon, M.; Dodd, J. H., Barrish, J. C.; Schieven, G. L.; Leftheris, K. Discovery of 4-(5-(Cyclopropylcarbamoyl)-2-methylphenylamino)-5-methyl-N-propylpyrrolo[1,2-*f*][1,2,4]triazine-carboxamide (BMS-582949), a Clinical p38α MAP Kinase Inhibitor for the Treatment of Inflammatory Diseases. *J. Med. Chem.* **2010**, *53*, 6629-6639.

[23] Salituro, F.; Bemis, G.; Cochran, J. Inhibitors of p38. Patent WO0017175, published March 30, 2000.

[24] Salituro, F.; Bemis, G.; Evindar, G. Pyridine derivatives as inhibitors of p38. Patent WO00170695, published September 27, 2001.

[25] Hill, R. J.; Dabbagh, K.; Phippard, D.; Li, C. Suttmann, R. T.; Welch, M.; Papp, E.; Song, K. W.; Chang, K.-C.; Leaffer, D.; Kim, Y.-N.; Roberts, R. T.; Zabka, T. S.; Aud, D.; Dal Porto, J.; Manning, A. M.; Peng, S. L.; Goldstein, D. M.; Wong, B. R. Pamapimod, a novel p38

mitogen-activated protein kinase inhibitor: preclinical analysis of efficacy and selectivity. *J. Pharmacol. Exp. Ther.* **2008**, *46*, 4676-4686.

[26] Kaieda, A.; Takahashi, M.; Takai, T.; Goto, M.; Miyazaki, T.; Hori, Y.; Unno, S.; Kawamoto, T.; Tanaka, T.; Itono, S.; Takagi, T.; Hamada, T.; Shirasaki, M.; Okada, K.; Snell, G.; Bragstad, K.; Sang, B. C.; Uchikawa, O.; Miwatashi, S. Structure-based Design, Synthesis, and Biological Evaluation of Imidazo[1,2-*b*]pyridazine-based p38 MAP Kinase Inhibitors. *Bioorg. Med. Chem.* **2018**, *26*, 647-660.

[27] Duffy, J. P.; Harrington, E. M.; Salituro, F. G.; Cochran, J. E.; Green, J.; Gao, H.; Bemis, G. W.; Evindar, G.; Galullo, V. P.; Ford, P. J.; Germann, U. A.; Wilson, K. P.; Bellon, S. F.; Chen, G.; Taslimi, P.; Jones, P.; Huang, C.; Pazhanisamy, S.; Wang, Y. M.; Murcko, M. A.; Su, M. S. The Discovery of VX-745: A Novel and Selective p38α Kinase Inhibitor. *ACS Med Chem Lett.* **2011**, *2*, 758-63.

[28] Lomas, D. A.; Lipson, D. A.; Miller, B. E.; Willits, L.; Keene, O.; Barnacle, H.; Barnes, N. C.; Tal-Singer, R. An oral inhibitor of p38 MAP kinase reduces plasma fibrinogen in patients with chronic obstructive pulmonary disease. *J. Clin. Pharmacol.* **2012**, *52*, 416−424.

[29] Watz, H.; Barnacle, H.; Hartley, B. F.; Chan, R. Efficacy and safety of the p38 MAPK inhibitor losmapimod for patients with chronic obstructive pulmonary disease: a randomised, double-blind, placebocontrolled trial. *Lancet Respir. Med.* **2014**, *2*, 63−72.

[30] See ClinicalTrials.gov (https://www.clinicaltrials.gov/ct2/home) to check the latest clinical information.

[31] Aguzzi, A.; Barres, B. A.; Bennett, M. L. Microglia: Scapegoat, saboteur, or something else? *Science* **2013**, *339*, 156-161.

[32] Gandy, S.; Heppner, F.L. Microglia as dynamic and essential components of the amyloid hypothesis. *Neuron*, **2013**, *78*, 575-577.

[33] Meraz-Rios, M.A.; Toral-Rios, D.; Franco-Bocanegra, D.; Villeda-Hernandez, J.; Campos-Pena, V. Inflammatory process in Alzheimer's Disease. *Front Integr Neurosci* **2013**, *7*, 59.

[34] Griffin, W. S. T. Neuroinflammatory cytokine signaling and Alzheimer's disease. *N Engl J Med.* **2013**, *368*, 770-771.

[35] Alam, J. J. Selective brain-targeted antagonism of p38 MAPKa reduces hippocampal IL-1b levels and improves Morris water maze performance in aged rats. *J. Alzheimer's Disease* **2015**, *48*, 219-227.

[36] Fitzgerald, C. E.; Patel, S. B.; Becker, J. W.; Cameron, P. M.; Zaller, D.; Pikounis, V. B.; O'Keefe, S. J.; Scapin, G. Structural basis for p38alpha MAP kinase quinazolinone and pyridol-pyrimidine inhibitor specificity. *Nat. Struct. Biol.* **2003**, *10*, 764–769.

[37] Koeberle, S. C.; Romir, J.; Fischer, S.; Koeberle, A.; Schattel, V.; Albrecht, W.; Grutter, C.; Werz, O.; Rauh, D.; Stehle, T.; Laufer, S. A., Skepinone-L is a selective p38 mitogen-activated protein kinase inhibitor. *Nat. Chem. Biol.* **2012**, *8*, 141-143.

[38] Goldstein, D. M.; Kuglstatter, A.; Lou, Y.; Soth, M. J. Selective p38r Inhibitors Clinically Evaluated for the Treatment of Chronic Inflammatory Disorders. *J. Med. Chem.* **2010**, *53*, 2345–2353.

[39] Hammach, A.; Barbosa, A.; Gaenzler, F. C.; Fadra, T.; Goldberg, D.; Hao, M.; Kroe, R. R.; Liu, P.; Qian, K. C.; Ralph, M.; Sarko, C.; Soleymanzadeh, F.; Moss, N. Discovery and design of benzimidazolone based inhibitors of p38 MAP kinase. *Bioorg. Med. Chem. Lett.* **2006**, *16*, 6316-6320.

10.1002/cmdc.201900129

Entry for the Table of Contents

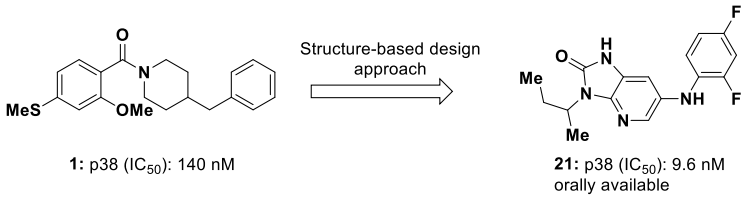

Scaffold hopping: High-throughput screening identified the carbonylpiperidine derivative as a hit compound of p38 MAP kinase inhibitors. Based on the X-ray crystallographic analysis of the complex of the hit with the enzyme, structure-based design has led to potent and orally available imidazo[4,5-*b*]pyridin-2-one-based p38 MAP kinase inhibitors.